DOI 10.1007/s11182-015-0573-y

Russian Physics Journal, Vol. 58, No. 6, October, 2015 (Russian Original No. 6, June, 2015)

TOPOLOGY OF WRINKLONS IN GRAPHENE NANORIBBONS IN THE VICINITY OF CONSTRAINED EDGE

E. A. Korznikova,[1] J. A. Baimova,[1] and S. V. Dmitriev[1,2] UDC 539.31

Most of the two-dimensional materials possessing low bending stiffness tend to lose the flat shape to form topological defects in the form of wrinkles and folds under the action of external factors. One of the striking examples of such material is graphene, where the presence of wrinkles leads to changes in physical, mechanical, and chemical properties of the material. Thus, changing the geometry of wrinkles, one can purposefully control properties of graphene. In this paper, we studied the characteristics of wrinkles appearing in graphene under the influence of elastic deformation, as well as the evolution of the configuration of wrinkles in the vicinity of the constrained edge of the graphene nanoribbon at different initial conditions. It is found that near the constrained edges of the deformed graphene nanoribbons, it is profitable to form wrinklons, that is, transition regions, where two or more wrinkles merge into one. The stability of two types of wrinklons formed by merging of the two or three wrinkles in one is shown. It is shown that in the process of the structure relaxation of the uniformly deformed graphene depending on the initial configuration of wrinkles, hierarchy of wrinkles containing wrinklons of one or another type is formed near the constrained edges. The results allow to explain the experimentally observed topology of the graphene sheet in the vicinity of the constrained edge.

Keywords: graphene, hierarchy of wrinkles, wrinklon, elastic deformation, molecular dynamics.

INTRODUCTION

Graphene is a two-dimensional crystal of carbon, where each atom is connected by covalent bonds with three nearest neighbors. Due to the presence of the delocalized covalent bond, graphene possesses unique electrical properties [1, 2] and high thermal conductivity [3]. Like many other two-dimensional materials, graphene has high strength and stiffness when stretched in the plane of the sheet [4–7], but it has very low bending stiffness, which leads to the formation of wrinkles and folds under the influence of external factors [8–16].

It was shown in [17] that the formation of wrinkles is often observed in two-dimensional materials. The properties of graphene depend strongly on the applied deformation and surface topology. Among the factors leading to the loss of the flat shape by the graphene sheet, we note the application of compressive stresses acting in the plane of the sheet [8–16], interaction with the substrate [18], partial hydrogenation [19], and thermal fluctuations [13, 14].

Formation of wrinkles in the graphene and graphene nanoribbons was investigated both experimentally and theoretically. The potential energy E and amplitude A of wrinkles depend on the wrinkles wavelength λ and obey the laws of $A \sim \lambda$ and $E \sim \lambda^{-2}$ over a wide range of the plane deformation of graphene [18, 20]. The wrinkle formation in the hanging two-dimensional materials was studied in [17], where it was shown that the structural instability due to the fixing of edges is the cause of the formation of quasi-periodic wrinkles. The wavelength of wrinkles increases, as the distance from the constrained edge x increases according to the law $\lambda \sim x^m$. This low is valid for most of the two-

[1]Institute for Metals Superplasticity Problems of the Russian Academy of Sciences, Ufa, Russia, e-mail: Elena.a.korznikova@gmail.com; Julia.a.baimova@gmail.com; Dmitriev.sergey.v@gmail.com; [2]National Research Tomsk State University, Tomsk, Russia. Translated from Izvestiya Vysshikh Uchebnykh Zavedenii, Fizika, No. 6, pp. 61–66, June, 2015. Original article submitted March 6, 2015.

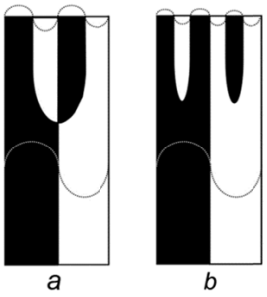

Fig. 1. Schematic representation of wrinklons, that is, transition regions of merging of the two wrinkles in one ($\lambda \rightarrow \lambda/2$, $\{1\rightarrow2\}$) (*a*) and of the three wrinkles in one ($\lambda \rightarrow \lambda/3$, $\{1\rightarrow3\}$) (*b*). Black and white areas of the nanoribbon show the positive and negative movements of atoms from the plane of the graphene sheet.

dimensional materials prone to wrinkling, regardless of the type and thickness of the material. The exponent m is in the range from 1/2 to 2/3 for different materials.

The term wrinklon first introduced by the authors of [17] denotes a zone, where several wrinkles merge in one. It was also shown that the hierarchy of wrinklons spontaneously arising in the two-dimensional material with the constrained edge is self-similar.

Figure 1 shows examples of merging of the two wrinkles in one ($\lambda \rightarrow \lambda/2$) (*a*) and of the three wrinkles in one ($\lambda \rightarrow \lambda/3$) (*b*). Hereinafter, these transitions are briefly designated by $\{1\rightarrow2\}$ and $\{1\rightarrow3\}$, respectively. Black and white areas of the nanoribbon show the positive and negative movements of atoms from the plane of the graphene sheet, respectively. Note that in Fig. 1*a*, there is a singular point, where two black and two white areas merge. There are no such points in Fig. 1*b*. Probably, metastable structures corresponding to the more complex transitions of k wrinkles in l can also be formed.

Due to the fact that controlled wrinkling is an effective way to influence the phonon and electron spectra of graphene, its chemical reactivity, optical properties, etc. [21], the study of special features of this process is an urgent task. In this paper, equilibrium configurations of wrinkles in the deformed graphene in the vicinity of the constrained edge are studied by the method of molecular dynamics under relaxation.

MODEL DESCRIPTION

The initial structure for simulation was constructed by translation of the graphene rectangular unit cell containing four carbon atoms. [22] Translational cells were numbered by indices m and n in the directions x and y, respectively (see Fig. 2). The x and y axes were chosen along the zigzag and armchair directions, respectively. During the relaxation, every atom in the calculated cell had three degrees of freedom (the components of the displacement vector). At the edges of the calculated region parallel to the y axis, periodic boundary conditions were used. The edges parallel to the x axis were firmly constrained (Fig. 2*a* shows the half width of the nanoribbon with upper constrained edge).

The nanoribbon width W (the calculated cell size in the y-axis direction) was N = 480–700 translational elementary cells, and the calculated cell size L in the x-axis direction was M = 56–150 cells. The simulation was performed at zero temperature.

To describe interatomic interactions, the potential proposed in [22] was used, which gives the equilibrium length of the valence bond $\rho_0 = 1.418$ Å. This potential has been successfully tested in finding the stability region of the graphene sheet uniformly deformed in its own plane [23], in studying the dynamics of motion of soliton waves in the deformed graphene [24], and in studying the discrete breathers in graphene and graphene nanoribbons [25-28].

In all considered cases, the nanoribbon was elastically deformed in the plane by the strain $\varepsilon_{xx} = -0.08$, $\varepsilon_{yy} = 0.1$. The compressive strain in the x-axis direction provided the appearance of wrinkles oriented along the y direction in the

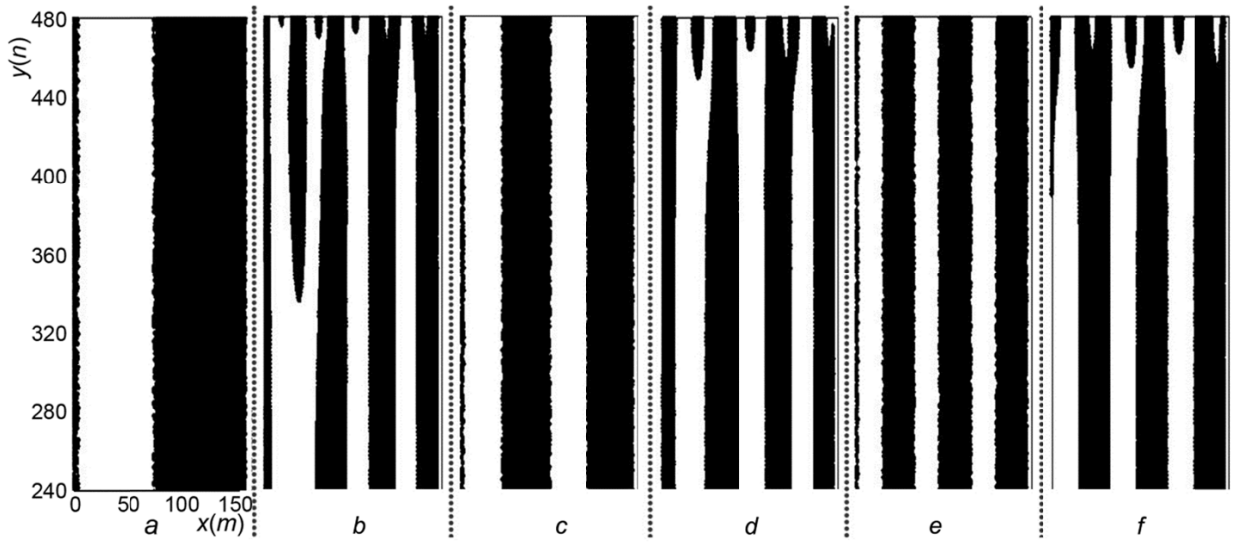

Fig. 2. Initial (*a*, *c*, *e*) configurations of the nanoribbon wrinkles and configurations formed after the relaxation (*b*, *d*, *f*). A half of the calculated area near the upper constrained edge (240 <*n* <480) is shown. Black (white) color corresponds to a positive (negative) displacement of atoms from the nanoribbon plane.

nanoribbon. To study the relaxation dynamics, the viscosity term was introduced in the equations of motion of atoms. Equilibrium configurations of nanoribbons of various widths with different initial conditions were studied.

The initial conditions were set in two different ways:

1. A nanoribbon with the width of $W = 2042$ Å ($N = 480$) and size of the calculated cell of $L = 339$ Å ($M = 150$) is considered (see Fig. 2). In the elastically deformed graphene nanoribbon, the displacements of atoms from the plane of the nanoribbon were set in the form of the function $\Delta z(x, y) = A\sin(2\pi x/\lambda)$ for $\lambda = L$, $L/2$, and $L/3$. The obtained initial configurations are shown in Fig. 2*a*, *c*, *e*. Positive and negative displacements of atoms of the nanoribbon are shown in black and white. For the wave amplitude of initial displacements from the plane, a sufficiently small value of $A = 0.3$ Å was chosen, to prevent the breaking of valence bonds near the constrained edge.

2. In the second case, a nanoribbon with the width $W = 2978$ Å ($N = 700$) and three various sizes of the calculated cell: $L = 126.56$, 180.8, and 235.04 Å corresponding to the numbers of elementary cells $M = 56$, 80, and 104 was considered. The initial conditions were set, to simulate the transition between the wrinkles in the graphene nanoribbons with different wavelengths. To this end, the displacements of atoms in the direction normal to the plane of the nanoribbon were given in the form of sinusoidal functions: $\Delta z\ (x, y) = A_1 \sin(2\pi x/\lambda_1)$ in the range $0 \le n \le 550$ and $\Delta z(x, y) = A_2 \sin(2\pi x/\lambda_2)$ in the range $551 \le n \le 699$, where $\lambda_1 = L$ and $\lambda_2 = L/2$ or $L/3$. The amplitudes of the initial displacements were $A_1 = A_2 = 0.15$ Å. The initial configurations for the transitions {1→2} and {1→3} are shown in Fig. 3*a* and *b*, respectively. Note that the topology of the initial conditions in Fig. 3*a* and *b* corresponds to the topology of structures shown in Fig. 1.

For both types of initial conditions, initial displacements of atoms in the plane of the graphene sheet and the initial velocities of atoms are zero.

SIMULATION RESULTS

Figures 2*b*, *d*, *f* show the configurations of wrinkles resulting from the relaxation of initial structures shown in Figs. 2*a*, *c*, *e*, respectively. It may be noted that the morphology of wrinkles formed as a result of relaxation weakly depends on their initial configurations. Thus, relaxation of the initial structure containing one wrinkle with $\lambda = L$ (Fig. 2*a*) leads to the formation of the hierarchy of wrinkles {3 → 4 → 9}, while moving from the middle of the

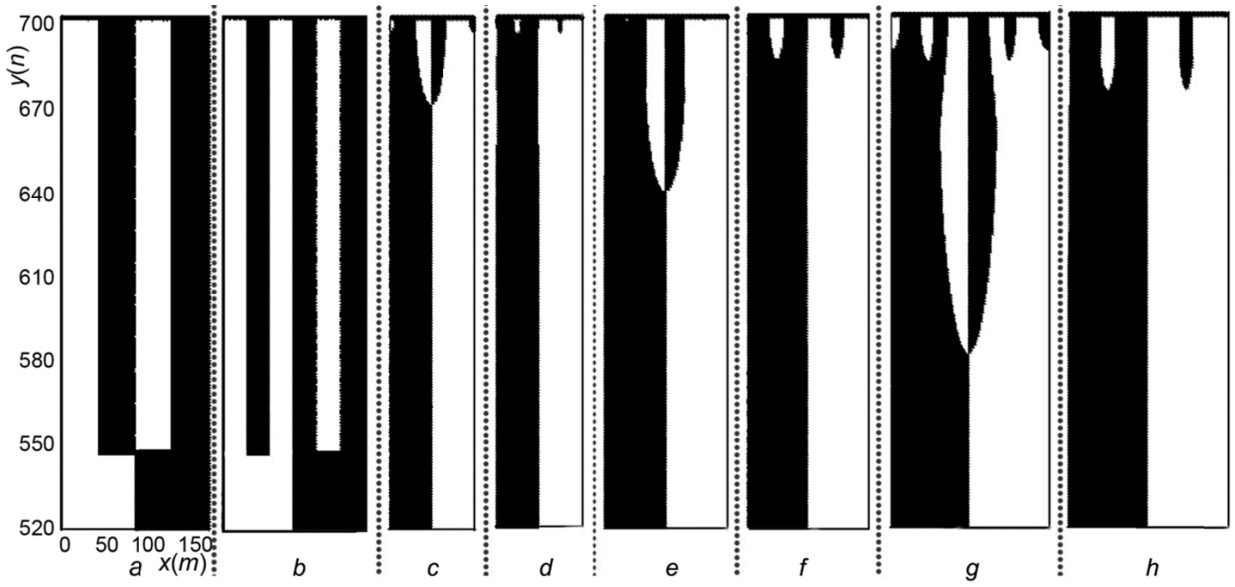

Fig. 3. Initial configurations of wrinkles {1→2} (*a*) and {1→3} (*b*) in the nanoribbons and configurations formed as a result of relaxation for the calculated areas of various sizes: *c*, *d* – L = 126.56 Å, *e*, *f* – L = 180.8 Å, *g*, *h* – L = 235.04 Å. For *c*, *e*, *g*, the transitions {1→2} are formed and for *d*, *f*, *h*, the transitions {1→3} are formed. Black (white) color corresponds to a positive (negative) displacement of atoms from the nanoribbon plane.

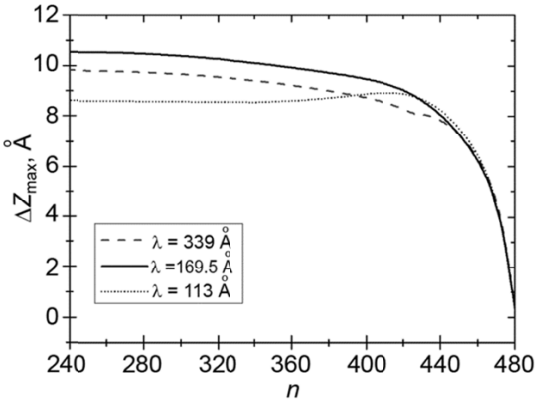

Fig. 4. Dependence of the maximum displacements from the plane (*xy*) on the number of the unit cell *n* for the structures shown in Fig. 2*b*, *d*, *f*. The number n = 480 corresponds to the constrained edge.

nanoribbon to the constrained edge (see Fig. 2*b*). The dependence of the maximum amplitude of wrinkles ΔZ_{max} on the number of the unit cell n near the constrained edge ($430 < n < 480$) shown in Fig. 4 is well approximated by a polynomial of the fourth order, which confirms the observations [22]. In the center of the nanoribbon, maximum displacement from the plane (*xy*) is about 10 Å.

The morphology of wrinkles observed during the relaxation of nanoribbons containing two wrinkles with $\lambda = L/2$ = 169.5 Å (Fig. 2*c*, *d*) is, in general, similar to that in the previous case. The hierarchy of the resulting structure can be described as {3→7} (Fig. 2*d*). As can be seen from Fig. 4, the maximum displacement amplitude is 10.5 Å.

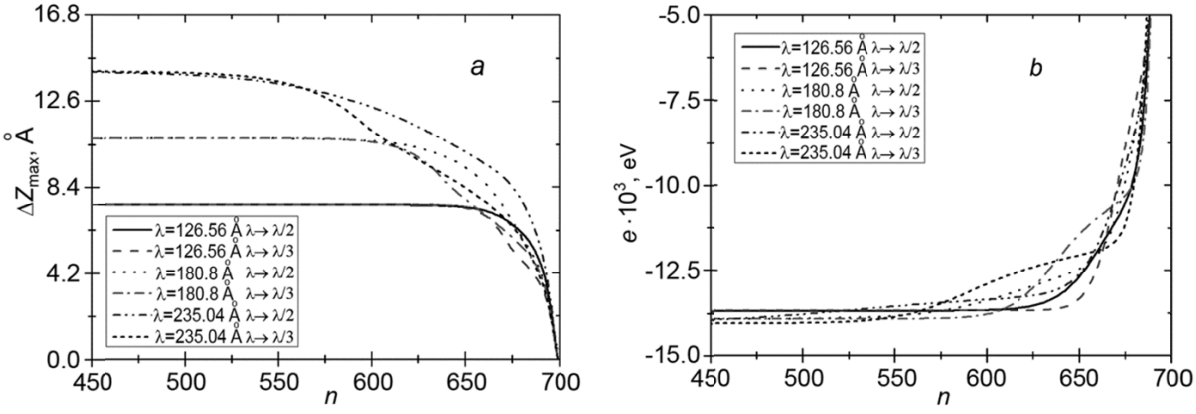

Fig. 5. Dependences of the maximum displacement from the plane (*xy*) (*a*) and the potential energy per atom (*b*) on the unit cell number *n* after relaxation for the structures shown in Figs. 3, *c*–*h*. The number $n = 700$ corresponds to the constrained edge.

In case of the initial structure with $\lambda = L/3 = 113$ Å (Fig. 2*e*, *f*), the transitions observed after the energy minimization can also be described as {3→7}. As seen from Fig. 4, the maximum amplitude of the displacements is 8.5 Å.

According to the results shown in Fig. 2, we can conclude that at a maximum distance from the constrained edge, the state with three wrinkles is advantageous within the periodicity cell, because the distance from the constrained edge is not large enough for them to merge into one wrinkle. Thus, it follows from [22] that with increasing distance from the constrained edge, an increase in the wavelength of wrinkles is observed. The displacements from the plane (*xy*) of the nanoribbon also increase as $\Delta Z \sim \Delta n^4$, where Δn corresponds to the distance from the constrained edge.

With increasing size of the nanoribbon in the direction *y*, a state can be achieved, where the configuration with one wrinkle becomes advantageous. It should also be noted that the spontaneously formed hierarchy of wrinkles contains only elementary transitions of {1→3} type schematically shown in Fig. 1*b*. In this case, no transitions {1→2} shown in Fig. 1*a*, are observed.

To analyze the possibility of realization and probability of formation of elementary transitions {1→2} and {1→3}, nanoribbons with initial conditions containing these transitions were investigated (Fig. 3*a*, *b*). As a result of the relaxation of the nanoribbon with the width $L = 126.56$ Å, the initial hierarchy of wrinkles {1→2} and {1→3} remains unchanged (Fig. 3*c*, *d*) and the length of the short-wave part of the nanoribbon significantly decreases, which is due to the fact that the existence of the long-wavelength configuration is energy favorable [29, 30].

It should also be noted that the case of the transition {1→3} is characterized by a much smaller length of the transition region. With the increase in width up to $L = 180.8$ Å, the topology of the relaxed structure remains unchanged, only the length of the transition region increases. From the plot of the dependence $\Delta Z_{max}(n)$ (Fig. 5*a*), it can be concluded that the length of the transition region near the constrained edge is increased approximately 2-fold. For the transitions {1→3}, the maximum amplitude decreases more smoothly, while approaching to the constrained edge, which is reflected in the lower level of energy in the corresponding areas (Fig. 5*b*).

Under the relaxation of nanoribbons with the transitions {1→2} and {1→3} and width $L = 235.04$ Å, the first one is transformed to the {1→5} type. In this case, the wrinklons newly formed near the edge of the nanoribbon relate to the {1→3} type. As in case of smaller *L*, the transition {1→3} is characterized by greater smoothness and lower energy in the corresponding area.

It was shown in [30] that in spite of the significant differences in the topology, the energy characteristics of both types of wrinklons are close to each other. The differences in the local increments of elastic strains $\Delta\varepsilon_{xx}$ and $\Delta\varepsilon_{yy}$ caused by the presence of the wrinklon have one order of magnitude. The transition of the {1→3} type is characterized by lower values of $\Delta\varepsilon_{xx}$ and $\Delta\varepsilon_{yy}$, than the transition {1→2}. This may be one of the reasons for the preferential

formation of a certain elementary type of the wrinklon under spontaneous formation of the wrinkle hierarchy shown in Fig. 2.

CONCLUSIONS

This paper deals with various structures of wrinkles and wrinklons appearing in the graphene nanoribbon with constrained edges uniformly deformed in its own plane. Two types of wrinklons are described: transition regions, within which several wrinkles merge in one, namely, transitions of the {1→2} and {1→3} types (Fig. 1). It is found that:

1) Relaxation of nanoribbons with the width W = 2042 Å (N = 480) and calculated cell size L = 339 Å (M = 150) (see Fig. 2) initially containing from one to three of wrinkles leads in all three cases to the formation of similar hierarchy of wrinkles near the constrained edges containing only the transitions {1→3} that are energetically favorable and cause lower local lattice distortions [30].

2) An analysis of the evolution of elementary transitions {1→2} and {1→3} in nanoribbons with different values of L showed that the length of the wrinklon monotonically increases with increasing L. For L = 235.04 Å, the relaxation of the structure leads to the formation of new wrinklons along the constrained edge, which is caused by the tendency to minimize total potential energy of the system. It should also be noted that under the relaxation of the initial {1→3} structure, the density of wrinklons decreases with increasing L. In case of {1→2}, the density of wrinklons increases due to the formation of new alternating transitions near the constrained edge.

3) The dependence of the amplitude of the maximum displacements from the plane (xy) near the constrained edge can be approximated by a polynomial of the fourth order (see Fig. 4 and Fig. 5*a*).

The data obtained indicate that the existence of different metastable configurations of wrinkles under the same conditions is possible.

Taking into account that many of properties of graphene depend on the configuration of wrinkles, the study of ways to control the topology of wrinkles and their evolution could potentially be useful in the development of new nano-devices based on graphene.

This work was partly supported (for KEA) by President Grant for young scientist support No. MK-5283.2015.2. JAB is grateful for financial assistance from Russian Science Foundation grant No. 14-13-00982. SVD gratefully acknowledges financial support from RFBR grant No. 14-02-97029 and Tomsk State University Academic D. I. Mendeleev Fund Program in 2015.

REFERENCES

1. A. K. Geim and K. S. Novoselov, Nature Mater., 183 (2007).
2. A. H. Castro Neto, F. Guinea, N. M. R. Peres, *et al*., Rev. Mod. Phys., **81**, 109 (2009).
3. B. Liu, C. D. Reddy, J. W. Jiang, *et al*., Appl. Phys. Lett., **101**, 211909 (2012).
4. A. M. Iskandarov, Y. Umeno, and S. V. Dmitriev, Letters on Materials, **1**, No. 4, 143–146 (2011).
5. S. V. Dmitriev, J. A. Baimova, A. V. Savin, and Yu. S. Kivshar, Comput. Mater. Sci., **53**, 194–203 (2012).
6. S. V. Dmitriev and J. A. Baimova, A. V. Savin, and Yu. S. Kivshar, JETP Lett., **93**, 571–576 (2011).
7. J. A. Baimova, S. V. Dmitriev, A. V. Savin, and Yu. S. Kivshar, Phys. Solid State, **54**, 866–874 (2012).
8. J. A. Baimova, K. Zhou, and B. Liu, Letters on Materials, **4**, No. 2, 96–99 (2014).
9. E. A. Korznikova, J. A. Baimova, S. V. Dmitriev, *et al*., Rev. Adv. Mater. Sci., **39**, No. 1, 92–98 (2014).
10. J. A. Baimova and K. Zhou, Letters on Materials, **3**, 139–142 (2012).
11. P. P. Azar, N. Nafari, and M. R. R. Tabar, Phys. Rev. B, **83**, 165434 (2011).
12. J. A. Baimova, B. Liu, S. V. Dmitriev, and K. Zhou, Phys. Status Solidi (RRL), **8**, 336–340 (2014).
13. M. Neek-Amal and F. M. Peeters, Phys. Rev. B, **82**, 085432 (2010).
14. S. Costamagna, M. Neek-Amal, J. H. Los, and F. M. Peeters, Phys. Rev. B, **86**, 041408 (2012).
15. J. A. Baimova, S. V. Dmitriev and K. Zhou, Phys. Rev. B, **86**, 035427 (2012).

16. J. A. Baimova, S. V. Dmitriev and K. Zhou, Phys. Status Sol. B, **249**, 1393– 1398 (2012).
17. H. Vandeparre, M. Pineirua, F. Brau, *et al*., Phys. Rev. Lett., **106**, 224301 (2011).
18. R. Miranda and A. L. Vazquez de Parga, Nature Nanotechnol., **4**, 549–550 (2009).
19. Z. F. Wang, Y. Zhang, and F. Liu, Phys. Rev. B, **83** 041403(R) (2011).
20. E. A. Korznikova, Fund. Probl. Sovrem. Mater., **11**, 22– 25 (2014).
21. C. Wang, Y. Liu, L. Li, *et al*., RSC Adv., **4**, 9395–9400 (2014).
22. A. V. Savin, Yu. S. Kivshar, and B. Hu, Phys. Rev. B, **82**, 195422 (2010).
23. J. A. Baimova and A. V. Savin, Letters on Materials, **1**, 171–175 (2011).
24. A. V. Savin and Yu. S. Kivshar, Letters on Materials, **1**, 3–6 (2011).
25. E. A. Korznikova, A. V. Savin, J. A. Baimova, *et al*., Pis'ma v Zh. Eksp. Tekh. Fiz., **96**, 238–242 (2012).
26. E. A. Korznikova, J. A. Baimova, and S. V. Dmitriev, Europhys. Lett., **102**, No. 6, 60004 (2013).
27. S. V. Dmitriev, Letters on Materials, **1**, No. 2, 78–83 (2011).
28. J. A. Baimova, S. V. Dmitriev, and K. Zhou, Europhys. Lett., **100**, 36005 (2012).
29. E. A. Korznikova and S. V. Dmitriev, J. Phys. D: Appl. Phys., **47**, 345307 (2014).
30. E. A. Korznikova and S. V. Dmitriev, Pis'ma v Zh. Eksp. Tekh. Fiz., **100**, 201–206 (2014).
31. Z. Wang and M. Devel, Phys. Rev. B, **83**, 125422 (2011).